Hydrogen production with CO_2 capture by coupling steam reforming of methane and chemical–looping combustion (SR-CLC) — Use of an iron-based waste product as oxygen carrier burning a PSA tail gas.

María Ortiz*, Pilar Gayán, Luis F. de Diego, Francisco García-Labiano, Alberto Abad, Miguel A. Pans and Juan Adánez

Department of Energy and Environment, Instituto de Carboquímica (C.S.I.C.)

Miguel Luesma Castán 4, 50018 Zaragoza, Spain

Phone number: +34 976 733 977

Fax number: +34 976 733 318

E-mail: mortiz@icb.csic.es

*Corresponding Author. Tel.: +34-976-733977; fax: +34-976-733318; E-mail address: mortiz@icb.csic.es (M.Ortiz)

Abstract

In this work it is analyzed the performance of an iron waste material as oxygen carrier for a chemical-looping combustion (CLC) system. CLC is a novel combustion technology with the benefit of inherent CO_2 separation that can be used as a source of energy for the methane steam reforming process (SR). The tail gas from the PSA unit is used as fuel in the CLC system.

The oxygen carrier behaviour with respect to gas combustion was evaluated in a continuous 500 Wth CLC prototype using a simulated PSA off-gas stream as fuel. Methane or syngas as fuel were also studied for comparison purposes. The oxygen

carrier showed enough high oxygen transport capacity and reactivity to fully convert syngas at 880 ºC. However, lower conversion of the fuel was observed with methane containing fuels. An estimated solids inventory of 1600 kg/MW_{th} would be necessary to fully convert the PSA off-gas to CO_2 and H_2O. An important positive effect of the oxygen carrier-to-fuel ratio up to 1.5 and the reactor temperature on the combustion efficiency was found.

A characterization of the calcined and after-used particles was carried out showing that this iron-based material can be used as oxygen carrier in a CLC plant since particles maintain their properties (reactivity, no agglomeration, high durability, etc.) after more than 111 h of continuous operation.

Keywords: Hydrogen, Steam Reforming, Chemical Looping Combustion, CO_2 Capture, Oxygen Carrier, Iron oxide.

1. Introduction

It is widely accepted today that carbon dioxide coming from fossil fuel combustion is the most important greenhouse gas contributing to global warming. One of the options to overcome anthropogenic greenhouse effect is the development of CO_2 capture and storage technologies from flue gases of power plants [1]. However, CO_2 capture technology applied to transport sector is more complex, being the use of H_2 as fuel one possible option to reduce the CO_2 emissions [2].

However, H_2 is an energy carrier that must be produced from a primary energy source. So, if H_2 is used as a CO_2-free energy carrier, it must be produced without net release of

CO_2, for example, from electrolysis of water using renewable energy sources or from fossil fuels with CO_2 capture and storage.

Nowadays, the most widely used technology for H_2 production is methane steam reforming [3]. In the steam reformer, syngas is obtained by reforming of methane with water:

$$CH_4 + H_2O \rightarrow CO + 3\ H_2 \qquad \text{(R1)}$$

Methane steam reforming (SR) is a mature technology used for decades and the hydrogen cost is less than hydrogen produced from renewable energy sources or from solid fossil fuels via gasification. The reforming reaction takes place in reformers tubes packed with a Ni catalyst. A possible alternative to conventional steam reforming of methane, is the autothermal reforming where the exothermic partial oxidation of methane is used as heat source for the reforming reaction [3]. In this process CH_4, H_2O and O_2 are fed together to an adiabatic reactor where both partial oxidation and reforming of methane happen. The main drawback of this process is the need of an air separation unit to produce the oxygen needed for the partial oxidation, which involves high energy consumption and costs.

The syngas produced is cooled and shifted in a water gas shift (WGS) reactor. In the WGS reactor the hydrogen production is maximized by conversion of CO by the WGS reaction. Usually, the WGS reaction is catalyzed by an iron-based catalyst to reduce the CO to around 2-5% at temperatures in the range of 400-500 ºC. At lower temperature (200-400 ºC) a copper-based catalyst is used to reduce the CO content to 1%. Next, the

hydrogen is separated from the other components in a pressure swing adsorption unit (PSA). After water removal, the PSA unit is able to recover between 75 to greater than 90% of the overall hydrogen in the syngas. The unrecovered H_2 is mixed with the rest of the gases coming from the WGS reactor. A typical PSA tail gas composition is 50-55 vol.% CO_2, 24-26 vol.% H_2, 15-20 vol.% CH_4, 0-2 vol.% CO and 0-5 vol.% H_2O depending on the operating parameters [4]. Usually, this gas stream is burned as fuel gas with air. In the most common configuration, the heat released during the combustion of PSA tail gas is used for the endothermic reforming reaction. To increase the heating value of the PSA tail, gas natural gas is often added.

Likely, the production of hydrogen via steam reforming of natural gas will continue to be the dominant technology for the next few decades, despite the appreciable amount of CO_2 released during the operation of such units. Therefore, the development of new concepts for H_2 production via SR, with reduced capital costs and CO_2 emissions, is extremely desirable.

To avoid the emission of the CO_2 to the atmosphere when the PSA tail gas is burned, the CO_2 can be captured by means of available post-combustion or oxyfuel technologies. In post-combustion technologies the CO_2 is separated from the flue gases usually with MEA (monoethanolamine) absortion. In oxyfuel technologies the combustion is carried out using oxygen instead of air. The oxygen must be separated from air, e.g. using a cryogenic air separation unit (ASU). These kinds of technologies imply high cost and energy penalty, which reduces the efficiency of H_2 production and increases the H_2 cost.

A new process for H_2 production by steam reforming coupled with CO_2 capture by chemical-looping combustion (SR-CLC) was proposed by Rydén and Lyngfelt [5]. This process uses the benefits of the chemical-looping combustion process (CLC) regarding the CO_2 capture by integrating a CLC unit with the widely used catalytic Steam Reforming method for H_2 production. CLC is a novel combustion technology with inherent separation of the greenhouse gas CO_2 that involves the use of an oxygen carrier, which transfers oxygen from air to the fuel avoiding the direct contact between them. Figure 1(a) shows a general scheme of the CLC process. CLC system is made of two interconnected reactors, designated as air and fuel reactors. In the fuel reactor, the fuel gas (C_nH_{2m}) is oxidized to CO_2 and H_2O by a metal oxide (MeO) that is reduced to a metal (Me) or a reduced form of MeO:

$$(2n + m)\ Me_xO_y + C_nH_{2m} \rightarrow (2n + m)\ Me_xO_{y-1} + n\ CO_2 + m\ H_2O \qquad (R2)$$

The reduced oxide is further transferred into the air reactor where it is oxidized with air, and the material regenerated is ready to start a new cycle:

$$Me_xO_{y-1} + ½\ O_2 \rightarrow Me_xO_y \qquad (R3)$$

Thus, the combustion of the fuel is split in two reactions, which are carried out in the air and fuel reactors. The total heat produced in the system is the same as in normal combustion with air, but with the benefit of the inherent CO_2 separation in the flue gases. The flue gas leaving the air reactor contains only N_2 and unreacted O_2. The exit gas from the fuel reactor contains only CO_2 and H_2O. After water condensation, almost pure CO_2 can be obtained with little energy lost for component separation.

Steam Reforming integrated with Chemical-Looping Combustion (SR-CLC) is a process where steam and hydrocarbons are converted into syngas using reformer tubes packed with catalyst, just as in a conventional tubular steam reforming unit. Figure 1(b) shows the schematic diagram of this process. The main difference respect to conventional steam reforming is that a CLC system is used as means to provide heat for the endothermic reforming reactions and to capture CO_2. The reformer tubes are located in the fuel reactor or in a fluidized bed heat exchanger connected to the chemical-looping system, a procedure which provides very favourable conditions for the important heat transfer operation.

For H_2 production, the SR-CLC unit is integrated with water-gas shift (WGS) and pressure swing adsorption (PSA) units. In the SR-CLC process, the PSA tail gas is used as fuel in the fuel reactor of the CLC system. A net heat balance shows that the combustion of the PSA tail gas can provide the sufficient heat needed for the reforming reaction of the methane. Figure 2 shows the power supplied by the combustion of the PSA tail gas and the power needed for the reforming of 1 mol/s of CH_4 as a function of the reforming efficiency. During calculations, it was assumed that the ratio $CO:H_2:CO_2$ was 1:1.4:2.5, being the fraction of CH_4 determined by the reforming efficiency. This gas composition was taken from calculations made in the CACHET Project [6] where a feasible PSA off-gas from SR was determined to be 12 % of CH_4, 18 % of CO, 25 % de H_2 and 45 % of CO_2. When the reforming efficiency is low, the power supplied by the combustion of the PSA tail gas is much higher than the power requirements for the reforming of methane. If the reforming efficiency increases, the thermal power of the PSA tail gas decreases. However, the net balance is positive up to reforming efficiency

close to 100%. In this case, the net balance is negative, but it is possible to add some methane as fuel gas together with the PSA tail gas in the fuel reactor to increase the thermal power of the gas. As in usual CLC system, the gas stream exiting from the fuel reactor contains only CO_2 and H_2O, being separated from nitrogen of air, which remains in the exhaust gas from the air reactor. Thus, in the SR-CLC process all carbon in methane is obtained in a CO_2 stream after water condensation.

Rydén and Lyngfelt [5] showed a preliminary reactor design in order to demonstrate the feasibility of the SR-CLC process. They concluded that the reactor dimensions seems reasonable, and the SR-CLC process has the potential to achieve higher selectivity towards H_2 than conventional SR plants because of the low temperature in the reactors and the high heat-transfer coefficient on the outside of the reformer tubes, which makes it possible to utilize more of the energy provided with the fuel for reforming, rather than for production of export steam. In short, the hybrid configuration SR-CLC process has the potential to provide hydrogen with high selectivity and almost 100% CO_2 capture without energy penalty. However to date, there are not experimental data about the performance of a CLC system using PSA tail gas as fuel.

An important factor for the development of the SR-CLC technology is the selection of an oxygen carrier with suitable properties: high reactivity rate and oxygen transference capacity, complete fuel conversion to CO_2 and H_2O, high resistance to attrition and sufficient durability to minimize losses of elutriated solid, negligible carbon deposition what would release CO_2 in the air reactor; good properties for fluidization (no presence of agglomeration), as well as good chemical performance in successive cycle reactions.

In addition, the cost of the oxygen carrier, environmental characteristics, and health aspects are also important.

Different metal oxides have been proposed in the literature as candidates for the CLC process. Among them, iron, nickel and copper have been selected as the most promising ones [7-9]. To develop an oxygen carrier for the process synthetic particles based on a metal oxide and a support has been prepared by several methods with high performance and stability [10-13]. However, another route of development is to find low-cost minerals or ores and waste products as oxygen carriers. So, it is interesting to study the use of industrial wastes as substitutes to synthetic oxygen carriers to reduce the costs and the environmental impacts.

Recently, natural iron-based ores such as ilmenite and iron ores from steel industry have attracted significant interest especially in CLC for solid fuels. Berguerand and Lyngfelt [14] examined ilmenite as oxygen carrier for CLC for solid fuels. They studied the behaviour of ilmenite in a 10 kW chemical-looping combustor using a petroleum coke as fuel. The fuel conversion achieved was not high enough due to the plant design; however ilmenite showed a good behaviour regarding fluidization, attrition and agglomeration. More recently Xiao et al. [15, 16] investigated the behaviour of an iron ore at high pressure in a fixed bed reactor using coal as fuel. The authors stated that this iron ore presented suitable properties to be used as oxygen carrier in a pressurized CLC process.

Ilmenite has also been studied as a possible oxygen carrier for CLC with gaseous fuels [17-20]. Ilmenite showed an adequate reactivity working with syngas as fuel, but the

conversion achieved working with CH_4 as fuel was relatively low. Further, a screening of natural ores and industrial products based on Fe and Mn as possible oxygen carries was carried out by the Lyngfelt's research group [21-24]. The materials were tested in a laboratory batch fluidized bed reactor using syngas and methane as fuel. The waste products showed high reactivity with syngas components but modest reactivity with methane. They achieved high methane conversion mixing the waste with a small amount of a Ni-based oxygen carrier [23].

The aim of this work was to analyze the behaviour of an iron waste from aluminium manufacture as an oxygen carrier for the SR-CLC process. Particle reactivity was evaluated in a TGA and oxygen carrier behaviour with respect to gas combustion was performed in continuous operation in a 500 W_{th} CLC prototype using a simulated PSA off-gas as fuel. As far as we know, this is the first time that the performance of a CLC system is proven using PSA off-gas as fuel. For comparison purposes, the behaviour of this material using methane or syngas as fuel gas was also studied.

The effect on the combustion efficiency of different operating conditions, such as fuel composition, oxygen carrier-to-fuel ratio, fuel reactor temperature and solids inventory has been determined in the continuous unit. Finally, a characterization of calcined and after-used particles was also performed to investigate the possible changes undergone of the oxygen carrier after continuous operation.

2. Experimental section

2.1. Oxygen carrier material

A waste product from the aluminium production was used as oxygen carrier. This waste product is called “sand process” or “sand fraction” and it is mainly composed of Fe_2O_3. The “sand process” is the coarse fraction (particles over 150 μm) of the principal waste product of the aluminium production, the red mud.

The waste product was supplied by Alcoa Europe-Alúmina Española S.A., and it does not have commercial use. In fact the disposal of red mud constitutes a significant proportion of the overall production cost of alumina due to its very large quantity generated, that can vary from 55-65% of the raw material processed [25]. The use of this material as oxygen carrier for the CLC process could reduce the cost associated to the oxygen carrier production together with providing a solution for the disposal of this waste.

The solid waste was heat treated in an oven at 1200 ºC during 6 hours in order to reach its maximum oxidized state and to increase its mechanical strength. The sintered solid was sieved to a size the range of 100-300 μm. Elemental analysis, determined in a ICP Jobin Ybon 2000, showed that the particles consisted of 67.4% Fe_2O_3, 21.3% Al_2O_3, 4.8% SiO_2, 5.6% TiO_2, 0.8% NaO_2 and 0.1% CaO.

The main physical and chemical properties of the calcined material are shown in Table 1. The oxygen transport capacity, R_{OC}, was defined as the mass fraction of oxygen that can be used in the oxygen transfer, in the case of Fe-based oxygen carriers it will be

different depending on the final oxidation state reached during the reduction reaction. However, only the transformation from hematite to magnetite (Fe_2O_3/Fe_3O_4) is suitable for industrial CLC systems. Thermodynamics data show that high selectivity to the complete combustion products, that is CO_2 and H_2O, is only reached for this transformation [26]. Further reduction to FeO or Fe should be avoided since high H_2 and CO concentrations at the outlet of the fuel reactor would be produced. In addition, oxidation of more reduced compounds as FeO or Fe could result in fluidization problems due to agglomeration phenomena [27].

2.2. Oxygen carrier characterization

Several techniques have been used to characterize physically and chemically the calcined and after-used oxygen carrier particles. The Fe_2O_3 content active for the CLC process was determined by complete reduction of the sample with hydrogen in TGA. The real density of the particles was measured with a Micromeritics AccuPyc II 1340 helium picnometer. The force needed to fracture a particle was determined using a Shimpo FGN-5X crushing strength apparatus. The mechanical strength was taken as the average value of at least 20 measurements. The surface area of the oxygen carrier was determined by the Brunauer-Emmett-Teller (BET) method by adsorption/desorption of nitrogen at 77 K in a Micromeritics ASAP-2020 (Micromeritics Instruments Inc.), whereas the pore volumes were measured by Hg intrusion in a Quantachrome PoreMaster 33.

The identification of crystalline chemical species was carried out by powder X-ray diffractometer Bruker AXS graphite monochromator. The oxygen carrier particles were

also analyzed in a scanning electron microscope (SEM) ISI DS-130 coupled to an ultra thin window PGT Prism detector for energy-dispersive X-ray (EDX) analysis.

2.3. Reactivity tests in TGA

The reactivity of the oxygen carrier was determined in a TGA, CI electronics type, described elsewhere [7]. For the experiments, the oxygen carrier was loaded in a platinum basket and heated to the set operating temperature in air atmosphere. After weight stabilization, the experiment was started by exposing the oxygen carrier to alternating reducing and oxidizing conditions. To avoid mixing of combustible gas and air, nitrogen was introduced for two min after each reducing and oxidizing period. The reactivity of the oxygen carrier was determined with three different reducing gases: CH_4, CO and H_2 at different temperatures (830, 880 and 950 ºC). The gas composition was 15 vol.% of the reducing gas. In the experiments with CH_4 a 20 vol.% H_2O was introduced to avoid carbon formation by methane decomposition. Steam was incorporated to the gas stream by bubbling through a water containing saturator at the selected temperature to reach the desired water concentration. Similarly, 20 vol.% CO_2 was introduced together with CO to avoid carbon formation by the Boudouard reaction. In all cases, nitrogen was used to balance. For oxidation reaction, 100% air was used as reacting gas.

The conversion of solids for the reduction reaction was calculated as:

$$X_r = \frac{m_{ox} - m}{R_{OC} m_{ox}} \qquad \text{(R4)}$$

m_{ox} being the mass of the fully oxidized solids, m the instantaneous mass of the sample and R_{OC} the oxygen transport capacity of solids for the transformation between Fe_2O_3 and Fe_3O_4, given by Table 1. The conversion for the oxidation reaction was calculated as $X_o = 1 - X_r$.

2.4. 500 W_{th} experimental facility

Figure 3 shows a schematic diagram of the 500 W_{th} continuous atmospheric CLC facility used in this work, which was designed and built at Instituto of Carboquimica (CSIC). The pilot plant was basically composed of two interconnected fluidized-bed reactors –the air and fuel reactors–, a riser for solids transport from the air reactor (AR) to the fuel reactor (FR), a solid valve to control the solids flow rate fed to the fuel reactor, a loop seal and a cyclone. This design allowed the variation and control of the solid circulation flow rate between both reactors.

The FR (1) consisted of a bubbling fluidized bed (0.052 m i.d.) with a bed height of 0.1 m. In this reactor the oxygen carrier particles are reduced by the fuel. Reduced oxygen carrier particles overflowed into the AR (3) through a U-shaped fluidized bed loop seal (2), to avoid gas mixing between fuel and air. The oxidation of the carrier took place at the AR, which consisted of a bubbling fluidized bed (0.05 m i.d.) with a bed height of 0.1 m, followed by a riser (4) of 0.02 m i.d. and 1 m height. The regeneration of the oxygen carrier happened in the dense bed part of the AR allowing residence times high enough for the complete oxidation of the reduced carrier. Secondary air could be introduced at the top of the bubbling bed to help particle entrainment. N_2 and unreacted O_2 left the AR passing through a high-efficiency cyclone (5) and a filter (9) before the stack. The oxidized solid particles recovered by the cyclone were sent to a solids

reservoir setting the oxygen carrier ready to start a new cycle. In addition, these particles avoid the leakage of gas between the FR and the riser. The regenerated oxygen carrier particles returned to the FR by gravity from the solids reservoir through a solids valve (7) which controlled the solids circulation flow-rate entering the FR. A diverting solids valve (6) located below the cyclone allowed the measurement of the solids flow rates at any time. Fine particles produced by fragmentation/attrition in the plant were recovered in the filters that were placed downstream of the FR and AR.

The prototype had several tools of measurement and system control. Thermocouples and pressure drop transducers located at different points of the plant showed the current operating conditions in the plant at any time.The gas outlet streams of the FR and AR were drawn to respective on-line gas analyzers to get continuous data of the gas composition. CH_4, CO, CO_2 were measured at the fuel reactor outlet via an NDIR analyzer (Maihak S710) together with H_2 using a thermal conductivity analyzer (Maihak S710/THERMOR). At the outlet of air reactor, CO and CO_2 were measured by an NDIR analyzer (Siemens/Ultramat 22P), and O_2 by a paramagnetic analyzer (Siemens/Oxymat 5E).

The total solids inventory in the system was about 1.7 kg of solid material. The temperature in the air reactor was always kept constant at about 950 ±15ºC. The inlet flow of fuel was 300 NL h^{-1}, it means that the inlet gas velocity in the fuel reactor was 17 cm s^{-1} at 880ºC and 16 cm s^{-1} at 830ºC. The inlet air flow in the AR was 720 NL h^{-1} as primary air and 150 NL h^{-1} as secondary air. Nitrogen was used to fluidized the bottom loop seal (45 NL h^{-1}). During the experimental work two different distributor plates in the FR were used. The difference was the height which the distributor plate

was located inside the FR, allowing working with two different amounts of solids in the FR. When the distributor with highest height was used the amount of solids in the FR was about 310 g and 620 g using the shortest distributor plate.

Table 2 shows a summary of the different operating conditions used in the tests. The effect of the fuel reactor temperature on the fuel conversion was analyzed working at 830ºC and 880ºC. Three different fuels were used during the experimental work: a simulated PSA off-gas, CH_4 and syngas. The composition of the simulated PSA off-gas fed to the FR was 12 % of CH_4, 18 % of CO, 25 % de H_2 and 45 % of CO_2 [6]. In most of experiments, the PSA off-gas was diluted with nitrogen. Under all operating conditions, the ratio of the constituent gases of the PSA off-gas, i.e. CH_4, H_2, CO, CO_2 was maintained constant. Two different CO/H_2 molar ratios (1 and 3) were also used, corresponding to typical gas compositions obtained in coal gasification processes. The syngas composition fed to the reactor for the different ratios was selected to fulfill the water-gas shift equilibrium (WGS) at the operating temperature, which was assumed achieved immediately at the inlet of the FR. Table 2 shows the WGS equilibrium composition of the different tests when PSA off-gas or syngas were fed to the reactor. No steam was added to the fuel reactor in neither of the experiments. The H_2O concentration present in the equilibrium corresponds to the WGS reaction. Experiments PSA-1 to PSA-6 were conducted using the PSA off-gas diluted in a 50 vol.% with nitrogen at 880 ºC. The tallest distributor plate was used in the FR, i.e. the solids inventory in the FR was about 310 g. In these experiments the oxygen carrier-to-fuel ratio was varied by changing the solids flow-rate (f_s). The oxygen carrier-to-fuel ratio (ϕ) was defined by Eq. (1), as:

$$\phi = \frac{F_{Fe_2O_3}}{bF_{Fuel}} \qquad (1)$$

$F_{Fe_2O_3}$ being the molar flow rate of the iron oxide and F_{Fuel} is the inlet molar flow rate of the fuel in the FR. The parameter b is the stoichiometric coefficient of the fuel gas mixture, calculated in Eq. (2) as:

$$b = \frac{4x_{CH_4} + x_{CO} + x_{H_2}}{x_{CH_4} + x_{CO} + x_{H_2}} \qquad (2)$$

Thus, the oxygen carrier-to-fuel ratio (ϕ) was defined as the ratio between the oxygen supplied and the oxygen needed to stoichiometrically react with the fuel flow. A value of the ϕ ratio equal to unity means that the oxygen supplied by the solids is exactly the stoichiometric oxygen to fully convert the fuel gas to CO_2 and H_2O.

In experiments PSA-1 to PSA-6 the oxygen carrier-to-fuel ratio was varied between 0.9 and 2.7. During these experiments, it was not possible to increase the ϕ ratio above this value because the limitation of the solids circulation flow-rate (f_s) through the solids valve, see (7) in Figure 3. To increase the value of the ϕ ratio, experiments PSA-7 to PSA-15 were carried out varying the flow of the PSA off-gas, but maintaining roughly constant the solids circulation flow-rate. To maintain the total flow of gas entering to the fuel reactor, the corresponding flow of nitrogen was added in every case. When the flow of PSA off-gas was varied, the oxygen carrier-to-fuel ratio, the solids inventory per MW_{th} (m^*_{FR}) and the gas concentration were varied simultaneously. To identify the parameter which had higher influence on the combustion efficiency, test PSA-23 was

performed by changing either the PSA off-gas flow or the solids circulation rate one at time. In addition, experiments at a lower temperature (830 ºC) were carried out at different ϕ ratios by varying the PSA off-gas flow, see experiments PSA-24 to PSA-26. Finally, experiments PSA-17 to PSA-22 were done increasing the amount of solids in the FR until 620 g using the shortest distributor plate (2.0 kg of total solid inventory). The concentration of the PSA off-gas was varied between 10 and 80%. In most of these experiments the solids circulation flow-rate was maintained roughly constant, thus the differences with previous experiments were due to the variation of the gas residence time in the FR.

Additional experiments were carried out using methane (M-1 to M-9) or syngas (S-1 to S-6) as fuel gases at 880 ºC or 830 ºC. Similarly to the experiments using PSA off-gas, different fuel gas concentrations were selected.

To evaluate the behaviour of the oxygen carrier during the combustion tests, the combustion efficiency η_c, defined in Eq. (3), was used as a key parameter. The combustion efficiency (η_c) was defined as the ratio of the oxygen consumed by the gas leaving the FR to that consumed by the gas when the fuel is completely burnt to CO_2 and H_2O. So, the ratio gives an idea about how the CLC operation is close or far from the full combustion of the fuel, i.e. η_c = 100%.

$$\eta_c = \frac{\left(2x_{CO_2} + x_{CO} + x_{H_2O}\right)_{out} F_{out} - \left(2x_{CO_2} + x_{CO}\right)_{in} F_{in}}{\left(4x_{CH_4} + x_{CO} + x_{H_2}\right)_{in} F_{in}} 100 \qquad (3)$$

F_{in} being the molar flow of the inlet gas stream, F_{out} the molar flow of the outlet gas stream, and x_i the molar fraction of the gas in the inlet or outlet gas stream.

3. Results and discussion.

3.1. Reactivity in TGA

The oxygen carrier must have sufficient reactivity to be able to fully convert the fuel gas, and the deactivation of the oxygen carrier during operation in a CLC system should be minimized. Reactivity tests of calcined and after-used oxygen carrier particles were carried out in the TGA. Figure 4 shows the reduction and oxidation conversions versus time curves obtained using H_2, CO and CH_4 as reacting gases, and pure air for the oxidation at 880ºC. The oxygen carrier exhibited very fast oxidation reaction, reaching a conversion of 90% in 10 s and full conversion of solids in less than 60 s. During the reduction reaction the oxygen carrier presented high reactivity with H_2 and CO, and low reactivity with CH_4 as reacting gas. These results agree with the ones obtained by Abad et al. [28,29] who determined that the reactivity of an iron-based oxygen carrier was higher using H_2 or CO than CH_4 as a reducing gas, and Leion et al. [18] and Adánez et al. [30] who observed the same behaviour with ilmenite, a natural mineral mainly composed by iron and titanium.

Figure 5 shows the effect of temperature on the reactivity of the material using methane as reacting gas. The experiments were carried out at 830, 880 and 950ºC. The highest reactivity was observed at 950ºC, and the lowest working at 830ºC. Small differencies were observed between reactivities of the carrier with CH_4 at 830 and 880ºC, but considerable differencies were observed when the temperature was increased up to 950

ºC. Thus, temperatures about 950 ºC would be desirable to show a high reactivity of the "sand process" material with methane, comparable to that showed for H_2 and CO.

Frequently, the rate index is used to compare the oxygen transference rate among different oxygen carriers [31]. The rate index is defined as a normalize rate at a gas concentration of 15 vol.%, expressed in % min^{-1} as

$$\text{Rate index} = 60 \cdot 100 \cdot R_{OC} \frac{dX}{dt} \quad (4)$$

From results showed in Figures 4 and 5 it was calculated that the rate index for the "sand process" material was 4.2 % min^{-1} for H_2, 3.1 % min^{-1} for CO and 1.5 % min^{-1} for CH_4 at 880 ºC. These values are similar to those obtained for ilmenite in a previous work [30]. Moreover, the rate index doubles when the temperature is increased up to 950 ºC for methane, being 3.2 % min^{-1}. This value is as high as the one determined for a highly reactive iron-based oxygen carrier prepared by freeze granulation [32]. So, this material could be considered as oxygen carrier regarding its relatively high reactivity and its low cost as a waste product.

3.2. Test in CLC 500 W_{th} pilot plant

Combustion tests under different operation conditions were conducted in the facility using the iron-based waste as the oxygen carrier. The effect of oxygen carrier-to-fuel ratio, temperature of the fuel reactor and the fuel composition on the combustion efficiency, η_c, was analyzed. PSA off-gas, methane or syngas were used as fuel gas during the experimental tests. The steady state for each operation condition was

maintained for at least 60 min. A total of about 121 h at hot conditions, of which 92 corresponded to combustion conditions were carried out. As it was shown in a previous section, two different solids inventories in the FR were used. A total of 111 h at hot conditions, with 80 h at combustion conditions, corresponds to experiments carried out using the same batch of oxygen carrier particles (1.7 kg). The gas product concentrations of the fuel and air reactors were measured by on line analyzers. These gases concentrations were used to make carbon, hydrogen and oxygen mass balances over the whole reactor system. For better comparison, the results are presented in N_2 free basis and/or dry basis.

To analyze the gas product distribution of the fuel and air reactors, the reactions happening with different contribution during the oxygen carrier reduction-oxidation with methane, CO and H_2 must be considered. Thus, the following reactions can take place in the fuel reactor:

Oxygen carrier reduction

$$12\ Fe_2O_3 + CH_4 \leftrightarrow 8\ Fe_3O_4 + CO_2 + 2\ H_2O \quad \text{(R5)}$$

$$3\ Fe_2O_3 + H_2 \leftrightarrow 2\ Fe_3O_4 + H_2O \quad \text{(R6)}$$

$$3\ Fe_2O_3 + CO \leftrightarrow 2\ Fe_3O_4 + CO_2 \quad \text{(R7)}$$

Methane decomposition

$$CH_4 \leftrightarrow C + 2\ H_2 \quad \text{(R8)}$$

Carbon gasification

$$C + H_2O \leftrightarrow CO + H_2 \quad \text{(R9)}$$

Boudouard reaction

$2\ CO \leftrightarrow C + CO_2$ (R10)

Water gas shift

$CO + H_2O \leftrightarrow CO_2 + H_2$ (R11)

And in the air reactor:

Oxygen carrier oxidation

$4\ Fe_3O_4 + O_2 \leftrightarrow 6\ Fe_2O_3$ (R12)

Carbon combustion

$C + O_2 \leftrightarrow CO_2$ (R13)

$C + ½\ O_2 \leftrightarrow CO$ (R14)

As an example, Figure 6 shows the temperature profiles and the gas product distribution in the FR and AR using PSA off-gas as fuel and operating conditions corresponding to test PSA-4. The outlet gas concentrations and the temperatures were uniform during the whole combustion time. Mass balances were found to be accurate by using the measurements of the analyzers from the AR and FR. The combustion efficiency reached in this operation conditions was around 80 %, with CO_2, CH_4, H_2 and CO measured at the outlet of the FR. It was measured a methane concentration around 2.7 vol % and a very small concentration of CO and H_2.

A suitable oxygen carrier should not promote the formation of solid carbon in the FR. Carbon deposited on particles could be transported to the AR, where combustion with oxygen will happen. In this case, CO_2 will be emitted from the AR, reducing the carbon capture efficiency of the chemical-looping combustor. Carbon deposition on particles could happen in the FR by methane decomposition (R8) and the Boudouard reaction (R10). In the CLC prototype, carbon formation was evaluated by measuring CO and CO_2 concentrations in the outlet from the AR. As there was not gas leakage from the FR to AR, any carbon containing gas present in the AR outlet should come from solid carbon following the oxygen carrier particles. These gases were never detected in the AR in any test. Thus, no losses in CO_2 capture were produced by carbon transfer to the AR.

3.2.1. Effect of the oxygen carrier-to-fuel ratio and solids inventory

The effect of oxygen carrier-to-fuel ratio on the combustion efficiency of the PSA off-gas was studied through two ways: varying the solids circulation flow-rate or varying the fuel proportion in the gas fed to the fuel reactor, i.e. the fuel flow. These experiments correspond to the PSA tests 1-6 and 7-15, respectively, showed in Table 2. In both cases all of the other experimental conditions were maintained constant. Figure 7 shows the effect of the ϕ value on the combustion efficiency. When the value of ϕ is changed varying the solids circulation rate -by means of the solid valve (7) in Figure 3- it can be seen that the combustion efficiency is maintained roughly constant at a value of 80% when the ϕ ratio was decreased from 2.7 to 1.6, and then decreases when the ϕ ratio is approaching to unity. This result agrees with results shown in a previous work [29], where it was shown that the average reactivity of particles in the reactor scarcely

changed when the variation of the solid conversion in the reactor, ΔX_s, was lower than 0.4-0.5, corresponding to $\phi > 1.5–2$ in the experiments carried out in this work. The variation of the solid conversion can be calculated as:

$$\Delta X_s = \eta_c / \phi \quad (5)$$

However, the average reactivity of particles in the fluidized bed strongly decreases when ΔX_s was increasing to the complete conversion of solids, which corresponds to values of the ϕ ratio close to unity. Thus, the lower conversion of gas reached at ϕ ratios close to unity is related to a decrease in the average reactivity as the oxygen carrier is being more converted.

The solids circulation flow-rate in the CLC facility was limited to values about 13 kg h^{-1}, which prevented us from working with values of ϕ higher than 2.7 using a PSA off-gas diluted to 50%. To work at higher values of ϕ, other experiments were carried out by varying the fuel concentration. Figure 7 also shows the combustion efficiency obtained for these tests (PSA-7 to PSA-15). It can be seen that the combustion efficiency hardly goes beyond 80%, even if the oxygen carrier-to-fuel ratio was as high as 16. So, the conversion of the fuel was not limited by the capability of the oxygen carrier to transfer oxygen because the available oxygen was exceeded in 16 times the required oxygen to convert the fuel to CO_2 and H_2O. In addition, as the value of the ϕ ratio increases, also the solids inventory per MW_{th} of fuel increases. Thus, the highest solids inventory was 4000 kg/MW_{th}. However, the maximum efficiency of combustion was about 80%, as it was pointed above. The slight increase in combustion efficiency, showed as the solids inventory increases, can be explained by the negative effect caused when the fuel

concentration in the inlet stream decreases. Combustion efficiency should decrease due to the dependency of the reaction rate with fuel concentration. Therefore, it was found that the positive effect of increase the solids inventory in the fuel reactor per MW_{th} of fuel gas, m^*_{FR}, on the combustion efficiency was similar to the negative effect of the decrease of the fuel concentration.

The effect of decreasing the fuel concentration was evaluated by comparing the combustion efficiency obtained in experiments PSA-19 and PSA-23, see Figure 7. In these experiments, the ϕ ratio and the solids inventory per MW_{th} were maintained constant, but the fuel concentration was 60 % and 30 %, respectively. The combustion efficiency was 87.0 % when the fuel concentration was 60 %, but decreased to 76.3 % when the fuel was diluted to 30 %. So, it was showed that the fuel concentration had a relevant effect on the combustion efficiency, and higher efficiencies would be obtained using a non-diluted PSA off-gas as fuel.

In addition, the effect of ϕ on the combustion efficiency was only noticeable when the ϕ ratio was increased from up to 1.5 approximately; a further increase of the ϕ ratio did not cause a relevant increase in the combustion efficiency. So it can be concluded that the solids inventory in the fuel reactor per MW of fuel have a high relevance on the combustion efficiency, whereas the solids circulation rate also became important at $\phi < 1.5$.

To analyze this effect more deeply, the solids inventory in the fuel reactor was increased up to 620 g (2.0 kg of total solid inventory) by changing the position of the distributor plate in the fuel reactor, tests PSA-17 to PSA-22. As noted in Figure 7, the increase in

solids inventory produced a significant increase in combustion efficiency due to longer gas residence time in the FR. However, complete fuel conversion was not reached. Therefore it would be necessary to increase further the gas residence time in the fuel reactor. By extrapolation of the results showed in this work, and considering plug flow of gas in the fuel reactor [28], a solid inventory of 1600 kg/MW_{th} would be necessary to fully convert a pure stream of PSA off-gas. This value is in line to those found in the literature [28] using a synthetic oxygen carrier based on iron where to convert natural gas 2500 kg/MW_{th} were referred and 1100 kg/MW_{th} to fully convert syngas.

3.2.2. Effect of fuel composition

The effect of the fuel composition was studied using three different fuels: PSA off-gas, CH_4 and syngas. Figure 8 shows the effect of the fuel composition on the combustion efficiency. Nearly full conversion of the fuel was reached when syngas was fed in the fuel reactor, whatever the ratio CO:H_2 used. The high reactivity of the "sand process" material with these gases, see Figure 4, is the responsible of these good results. However, very low methane combustion efficiencies were found due to the low reactivity of this material at 880 ºC, as it was mesured in TGA, see Figure 4.
The combustion efficiencies increased when PSA off-gas was used as fuel, since PSA off-gas content 43 vol. % of CO+H_2, gases that react faster than methane with this waste material.

Figure 9 shows the effect of the oxygen carrier-to-fuel ratio on the gas product concentration measured at the outlet of the fuel reactor in dry and N_2 free basis when PSA off-gas, CH_4 or syngas was used as fuel. In all cases, a decrease in the value of ϕ

produces a decrease in the combustion efficiency due to an increase in the amount of unconverted gases at the outlet of the fuel reactor, i.e. CH_4, H_2 and CO. When syngas was used as fuel gas, the concentration of unconverted gases, here H_2 and CO, were low, indicating almost full conversion to CO_2 and H_2O. In the same way, H_2 and CO concentrations were low when PSA off-gas or methane were used as fuel. In these cases, methane was the main unconverted gas, due to the low reactivity of the "sand process" material with this gas. Therefore, the low conversion of methane is the main responsible of the low combustion efficiencies obtained in this work, even working at high oxygen carrier-to-fuel ratios.

3.2.3. Effect of the fuel reactor temperature

The effect of fuel reactor temperature was tested working at 880 and 830 ºC, using PSA off-gas or CH_4 as fuel. Figure 10 shows the effect of the fuel reactor temperature on the combustion efficiency, using the two fuels. It was found that an increase in the fuel reactor temperature produced an increase in the combustion efficiency as a consequence of higher oxygen carrier reactivity with both fuels. This effect was more significant for methane than for PSA off-gas. So, to achieve high combustion efficiencies, it would be necessary to work at higher FR temperatures. An increase of temperature to 950 ºC produced an important increase in the reactivity of the "sand process" material with methane, as it was shown in Figure 5. Unfortunately, it was not possible to increase the temperature in the fuel reactor above 880 ºC because of heat losses in the experimental facility. Thus, it is expected that high conversion of PSA off-gas could be reached working at higher temperatures, and even lower solid inventories per MW_{th} would be required to fully convert the fuel.

Another option to increase the combustion efficiency would be to improve the reactivity of the oxygen carrier with methane. This improvement could be achieved by mixing this iron-based waste with a small amount of a high reactive material. In recent years, several studies [23, 33, 34] have demonstrated that the reactivity of iron oxide with methane can be increased if a small amount of nickel oxide is introduced This is because the reduced Ni^0 catalyzes the decomposition of CH_4 into CO and H_2 which reacts faster with Fe_2O_3 than methane. In any case, any process involving mixtures of different types of oxygen carriers, one less reactive but cheap and another high reactive but risky, may required more extensive monitoring and regulation compared to processes using only iron-based oxygen carriers.

3.2.4. Oxygen carrier behaviour

A total of about 121 h at hot conditions, of which 92 h corresponded to combustion conditions, were carried out in continuous operation. It must be pointed out that after this operation time the oxygen carrier particles never showed agglomeration or defluidization problems.

As it was shown in previous sections, two different solids inventories in the CLC continuous plant were used. A batch of particles of 1.7 kg was used during 111 h in hot conditions, with 80 h at combustion conditions, without replacement or adding new material. During this operation, different solid samples were taken from the cyclones and filters to study the variation in their physical and chemical properties. The evolution of the textural and structural properties of the oxygen carriers were studied by different

techniques. Table 1 shows the main properties of this batch of used oxygen carrier particles and were compared to those of calcined particles. The BET specific surface area of the particles shows a small increase, but its value remains very low. The real density of the used particles presented a small decrease related with the slightly increase of the carrier porosity. These features suggest that some accumulative thermal sintering was occurring in the oxygen carrier particles during the operation in the CLC prototype.

The powder XRD patterns of the used carrier revealed the presence of the same compounds that in calcined particles, indicating the stability of the main inert oxides present in the material (Al_2O_3 and SiO_2). No other iron phases than hematite and magnetite were found in the different samples analyzed during operation coming from the fuel and air reactor. Hematite was found in samples extracted from the air reactor, whereas magnetite also appears in samples taken from the fuel reactor. This fact indicates that full oxidation of the oxygen carrier was performed in the air reactor.

The oxygen carrier particles were also analyzed by SEM-EDX. Figure 11 shows SEM images of carrier particles, calcined and after operation. As shown in Figures 11(a) and (b), the oxygen carrier particles exhibited an irregular shape and the general appearance of the used particles was similar to the calcined particles. No changes in the surface texture and the solid structure of the used particles were detected, compared to calcined particles; see Figures 11(c) and (d). The iron distribution inside the particles was analyzed by EDX in some particles embedded in resin epoxy, cut, and polished. It was found a uniform distribution of iron through the particles and there was not evidence of redistribution or migration during the redox cycles after comparing Figures 11(g) and (h). Here, it must be pointed out, that it was observed an external layer around some

calcined and used particles. The EDX showed that in both, calcined and used oxygen carrier particles, the external layer were aluminium-enriched while the rest of the particle was iron-enriched.

Moreover, no signs of agglomeration were observed in SEM pictures for used particles, agreeing with the avoidance of defluidization problems in the CLC prototype.
A slightly decreased of the mechanical strength of the particles, from 2.9 N to 2.1 N, was observed after operation during 111 h at high temperatures. An oxygen carrier with high attrition and/or fragmentation of particles can be a problem during operation in CLC. Particles elutriated from the fluidized bed reactors during operation were recovered in the cyclones and filters. The generation of fine particles was high at the beginning of the operation, and a decreasing mass of fines were recovered during the continuous operation. This fact was attributed to the high amount of fines particles present in the calcined oxygen carrier, in spite of particle sieving upper 100 μm. As it was explained in the experimental section, the waste material was first calcined to increase the mechanical strength of the particles. Fines were sticky to higher size particles during the thermal treatment, as can be seen in Figure 11(a). However, an accurate sieving followed by the heat treatment of the waste material could solve the high fines quantity recovered during operation. Nevertheless, the measured mechanical strength of the used particles was found high enough to fluidization operation and SEM images confirm that particles maintain their structural integrities and homogeneity, see Figure 11(d).

Since in every cycle of the CLC process the oxygen carrier undergoes important chemical and structural changes at high operating temperature, substantial changes in

the reactivity with the number of cycles might be expected. The reactivity of the used oxygen carrier particles at different operation times was analyzed by TGA. A gas composed of 15 vol.% CH_4 and 20 vol.% H_2O for the reduction and pure air for the oxidation were used at 950 ºC. Figure 5 shows the conversion versus time for the reduction and oxidation reaction of the used particles compared to the calcined ones. As can be seen, the reduction and oxidation reactivities of the oxygen carrier barely varied after its operation in the CLC prototype. Indeed, a slight increase in the reactivity both for oxidation and reduction reaction can be seen. Moreover, the Fe_2O_3 content of the used particles was also determined by complete reduction of the sample with hydrogen in TGA. The iron content and activity in the oxygen carrier remains constant, maintaining the oxygen transport capacity of the material at 2.4 wt.%, as it was shown in Table 1.

The analysis carried out to the particles demonstrated that this iron-based material can be used as oxygen carrier in a CLC plant because solid particles maintains its properties after more than 111 h of continuous operation (reactivity, no agglomeration, high durability, etc.).

4. Conclusions

An iron-based waste from the aluminium manufacture, called “sand process”, was evaluated as oxygen carrier for CLC combustion of PSA off-gas. Reactivity of the material was evaluated in TGA for reduction with H_2, CO and CH_4 and oxidation in air. High reactivity of this material for CH_4, H_2, CO and O_2 was observed at 950 ºC, but noticeable lower reactivity was shown for CH_4 at lower temperatures.

In addition, continuous operation in a CLC facility was performed during 121 h using a simulated PSA off-gas as fuel. Methane or syngas were also used as fuel for comparison purposes.

The oxygen carrier showed enough high oxygen transport capacity (2.4 wt.%) and reactivity to be able to fully convert a simulated syngas to CO_2 and H_2O at 880 ºC. However, lower conversion of the fuel was observed with methane containing fuels because the lower reactivity of this gas compared to CO and H_2. The combustion efficiency was about 75-80% when the solids inventory in the fuel reactor was 400 kg/MW_{th}, and increased until ~90% with 800 kg/MW_{th}, being the reactor temperature 880 ºC in all cases. At this condition, it was estimated that a solids inventory of 1600 kg/MW_{th} would be necessary to fully convert the PSA off-gas to CO_2 and H_2O. The effect of oxygen carrier-to-fuel ratio and the reactor temperature on the combustion efficiency was also analyzed. The combustion efficiency increases as the oxygen carrier-to-fuel ratio increases up to 1.5, and later remaining roughly constant. In addition, it was observed a notable increase in the combustion efficiency when the temperature increases, due to higher oxygen carrier reactivity.

Different alternatives to increase the combustion efficiency and to reduce the solids inventory were postulated as increasing the fuel reactor temperature or the addition of small amounts of highly reactive materials.

Important changes in the reactivity, surface texture and the solid structure of the oxygen carrier particles were not detected after more of 111 h of operation with the same batch of "sand process" particles. In addition, the oxygen carriers did not show agglomeration

or defluidization problems and the crushing strength of solid particles was maintained enough high for operation in a fluidized-bed reactor. Thus, the “sand process” material showed good performance during CLC operation to be considered as oxygen carrier.

Acknowledgments

This work was partially supported by the Spanish Ministry of Science and Innovation (MICINN) (CTQ2007-64400). M. Ortiz thanks Diputación General de Aragón for the F.P.I. fellowship. M.A. Pans thanks MICINN for the FPI fellowship. The authors also thank to Alcoa Europe-Alúmina Española S.A. for providing the solid material used in this work.

References

[1] IPCC special report on carbon dioxide capture and storage. In: Metz B, Davidson O, de Coninck HC, Loos M, Meyer LA, editors. Working group III of the intergovernmental panel on climate change. Cambridge University; 2005.

[2] M. Ball, M. Wietschel, Int. J. Hydrogen Energy 34 (2009) 615-627.

[3] J.R. Rostrup-Nielsen. Production of synthesis gas. Catal. Today 18 (1993) 305-324.

[4] S. Reddy, S. Vyas. Energy Procedia 1 (2009) 149-154.

[5] M.Rydén, A.Lyngfelt, Int. J. Hydrogen Energy 31 (2006) 1271-1283.

[6] Final report. CACHET project (FP VI-019972).

[7] J. Adánez, L.F. de Diego, F. García-Labiano, P. Gayán, A. Abad and J.M. Palacios. Energy Fuels 18 (2004) 371-377.

[8] P. Cho, T. Mattisson, A. Lyngfelt. Fuel 83 (2004) 1215–1225.

[9] Q. Zafar, T. Mattisson, B. Gevert. Energy Fuels 20 (2006) 34-44.

[10] P. Gayán, C. Dueso, A. Abad, J. Adánez, L.F. de Diego, F. García-Labiano. Fuel 88 (2009) 1016-1023.

[11] T. Mattisson, M. Johansson, A. Lyngfelt. Fuel 85 (2006) 736-747.

[12] M. Ishida, M. Yamamoto, T. Ohba. Energy Convers. Manage. 43 (2002) 1469-78.

[13] P. Erri, A. Varma. Chem. Eng. Sci. 62 (2007) 5682-87.

[14] N. Berguerand, A. Lyngfelt, Int. J. Greenhouse Gas Control 2 (2008) 169-179.

[15] R. Xiao, Q. Song, S. Zhang, W. Zheng, Y. Yang, Energy Fuels 24 (2010) 1449-1463.

[16] R. Xiao, Q. Song, M. Song, Z. Lu, S. Zhang, L. Shen. Combust. Flame 157 (2010) 1140-1153.

[17] T. Proll, K. Mayer, J. Bolhàr-Nordenkampf, P. Kolbitsch, T. Mattisson, A. Lyngfelt, H. Hofbauer, Energy Procedia 1 (2009) 27-34.

[18] H. Leion, A. Lyngfelt, M. Johansson, E. Jerndal, T. Mattisson, Chem. Eng. Res. Des. 86 (2008) 1017-1026.

[19] M. M. Azis, E. Jerndal, H. Leion, T. Mattisson, A. Lyngfelt, Chem. Eng. Res. Des. doi:10.1016/j.cherd.2010.03.006

[20] A. Cuadrat, A. Abad, J. Adánez, L.F. de Diego, F. García-Labiano, P. Gayán. 4th International Conference on Clean Coal Technologies, Dresden, Germany, 2009.

[21] H. Leion, T. Mattisson, A. Lyngfelt, Energy Fuels 23 (2009) 2307-2315**.**

[22] H. Leion, E. Jerndal, Britt-Marie Steenari, S. Hermansson, M. Israelsson, E. Jansson, M. Johnsson, R. Thunberg, A. Vadenbo, T. Mattisson, A. Lyngfelt, Fuel 88 (2009) 1945-1954.

[23] M. Rydén, E. Cleverstam, A. Lyngfelt, T. Mattisson, Int. J. Greenhouse Gas Control 3 (2009) 693-703.

[24] E. Jerndal, H. Leion, T. Mattisson, A. Lyngfelt. 1st International Conference on Chemical Looping, Lyon, France, 2010.

[25] R.K. Paramguru, P.C. Rath, V.N. Misra. Miner. Process. Extr. Metall. Rev. 26 (2005) 1-29.

[26] E. Jerndal, T. Mattisson, A. Lyngfelt. Chem. Eng. Res. and Des. 84 (2006) 795-806.

[27] P. Cho, T. Mattisson, A. Lyngfelt. Ind. Eng. Chem. Res. 45 (2006) 968-977.

[28] A. Abad, T. Mattisson, A. Lyngfelt, M. Johansson. Fuel 86 (2007) 1021-1035.

[29] A. Abad, J. Adánez, F. García-Labiano, L. F. de Diego, P. Gayán, J. Celaya, Chem. Eng. Sci. 62 (2007) 533-549.

[30] J. Adánez, A. Cuadrat, A. Abad, P. Gayán, L. F. de Diego, F. García-Labiano. Energy Fuels 24 (2010) 1402-1413.

[31] M. Johansson, T. Mattisson, A. Lyngfelt. Thermal Science 10 (2006) 93-107.

[32] T. Mattisson, M. Johansson, A. Lyngfelt. Energy Fuels 18 (2004) 628-637.

[33] M. Johansson, T. Mattisson, A. Lyngfelt, Energy Fuels 20 (2006) 2399-2407.

[34] M. Rydén, E. Cleverstam, M. Johansson, A. Lyngfelt, T. Mattisson. AIChE J. 56 (2010) 2211-2219.

Captions for the Figures

Figure 1. Schematic diagram of (a) CLC and (b) SR-CLC

Figure 2. Power required for the reforming of methane and power supplied by combustion of the PSA tail gas as a function of the reforming efficiency. The ratio $CO:H_2:CO_2$ was assumed to be 1:1.4:2.5. The fraction of CH_4 was determined by the reforming efficiency.

Figure 3. Schematic diagram of the 500 W_{th} Chemical-Looping Combustion facility.

Figure 4. Conversion versus time curves of calcined oxygen carrier using H_2, CO or CH_4 as reacting gases for reduction period and air during oxidation period. T = 880 ºC.

Figure 5. Conversion vs. time curves of the calcined oxygen carrier at several reacting temperatures and conversion curve at 950 ºC for particles after 111 h in the CLC facility. Reacting gas for reduction period: 15 vol.% CH_4, 20 vol.% H_2O, nitrogen to balance. Oxidation by air.

Figure 6. Temperature and gas product distribution at the outlet of AR and FR during a typical experiment. Experimental test PSA-4: T_{FR} = 880ºC, T_{AR} = 940ºC, PSA off-gas = 50 vol %, f_S = 6.6 kg h^{-1}, ϕ = 1.6.

Figure 7. Effect of the oxygen-to-fuel ratio on the combustion efficiency in the fuel reactor. T=880ºC, PSA off-gas. Solids inventory in the fuel reactor 310 g: (■) variation of the solids circulation rate, (□) variation of the fuel flow. (▲) Experiment PSA-23. Solids inventory in the fuel reactor 620 g: (∆) variation of the fuel flow.

Figure 8. Effect of the fuel composition on the combustion efficiency. T=880ºC. (●) CH_4, (■) PSA off-gas, (▲) Syngas CO/H_2= 1, (∆) Syngas CO/H_2= 3.

Figure 9. Effect of the oxygen carrier-to-fuel ratio on the outlet gas of the FR using as fuel (a) PSA off-gas, (b) CH_4, and (c) syngas. T = 880ºC. (▲) CH_4, (●) H_2, (□) CO.

Syngas: Empty dots: CO/H_2= 3, Filled dots: CO/H_2= 1. Gas concentrations are in dry basis and nitrogen free.

Figure 10. Effect of the fuel reactor temperature on the combustion efficiency. PSA off-gas: (●) T=830 ºC, (○) T=880 ºC. CH_4: (■) T=830 ºC, (□) T=880 ºC.

Figure 11. SEM-EDX images of the oxygen carrier particles both fresh (left) and after 111 h of operation (right); (a) and (b) SE (secondary electrons) image of the particles; (c) and (d) BSE (back-scattering electrons) photograph of a particle; (e) and (f) BSE image of a cross section of a particle; (g) and (h) EDX line profiles of Fe and Al in a cross section of a particle.

Table 1. Characterization of the calcined and after-used oxygen carrier particles.

	Calcined	**After used[(a)]**
Fe_2O_3 content (wt%)	71	71
Crushing strength (N)	2.9	2.1
Oxygen transport capacity, R_{OC} (%)[(b)]	2.4	2.4
Porosity (%)	23	30
Real density (g/cm^3)	4.3	4.1
Specific surface area, BET (m^2/g)	0.4	0.7
XRD main phases	Fe_2O_3, β-Al_2O_3, SiO_2	Fe_2O_3, β-Al_2O_3, SiO_2

[(a)] 111 h in 500 W_{th} CLC unit
[(b)] $R_{OC} = (m_{ox}-m_{red})/m_{ox}$

Table 2. Operating conditions and main data for the experiments carried out in the continuous CLC facility.

Test	T_{FR}	ϕ	Fuel gas[(a)]	Equilibrium concentraion (vol.%)					f_s	Power	m^*_{FR}
			(vol.%)	CH_4	%CO	$\%H_2O$	$\%CO_2$	$\%H_2$	(kg h^{-1})	W_{th}	(kg/MW)
PSA off-gas											
Variation of solids circulation rate (f_s)											
PSA-1	880	0.9	50	6.0	15.8	6.8	15.7	5.7	3.8	387	800
PSA-2	880	1.0	50	6.0	15.8	6.8	15.7	5.7	4.1	387	800
PSA-3	880	1.3	50	6.0	15.8	6.8	15.7	5.7	5.3	387	800
PSA-4	880	1.6	50	6.0	15.8	6.8	15.7	5.7	6.6	387	800
PSA-5	880	2.2	50	6.0	15.8	6.8	15.7	5.7	9.0	387	800
PSA-6	880	2.7	50	6.0	15.8	6.8	15.7	5.7	11.1	387	800
Variation of fuel gas concentration											
PSA-7	880	1.3	100	12.0	31.7	13.7	31.4	11.3	11.1	773	400
PSA-8	880	2.2	60	7.2	19.0	8.2	18.8	6.8	10.7	463	667
PSA-9	880	3.5	40	4.8	12.7	5.5	12.5	4.5	11.5	309	1000
PSA-10	880	4.1	40	4.8	12.7	5.5	12.5	4.5	13.6	309	1000
PSA-11	880	6.4	20	2.4	6.3	2.7	6.3	2.3	10.7	156	2000
PSA-12	880	8.3	20	2.4	6.3	2.7	6.3	2.3	13.6	154	2000
PSA-13	880	6.7	20	2.4	6.3	2.7	6.3	2.3	11.1	154	2000
PSA-14	880	13.0	10	1.2	3.2	1.4	3.1	1.1	10.7	77	4000
PSA-15	880	16.7	10	1.2	3.2	1.4	3.1	1.1	13.8	77	4000
Higher solids inventory in FR											
PSA-17	880	1.2	80	9.6	25.3	10.9	25.1	9.0	7.9	619	1000
PSA-18	880	1.7	70	8.4	22.2	9.6	22.0	7.9	9.8	541	1144
PSA-19	880	1.9	60	7.2	19.0	8.2	18.8	6.8	9.2	309	1333
PSA-20	880	2.4	50	6.0	15.8	6.8	15.7	5.7	9.8	387	1600
PSA-21	880	5.6	20	2.4	6.3	2.7	6.3	2.3	9.2	387	4000
PSA-22	880	11.2	10	1.2	3.2	1.4	3.1	1.1	9.2	77	8000
Variation of solids circulation rate and power											
PSA-23	880	2.0	30	3.6	9.5	4.1	9.4	3.4	5.0	232	1333
Lower FR temperature											
PSA-24	830	3.5	40	4.8	12.7	5.5	12.5	4.5	11.7	309	1000
PSA-25	830	7.4	20	2.4	6.3	2.7	6.3	2.3	12.3	154	2000
PSA-26	830	14.2	10	1.2	3.2	1.4	3.1	1.1	11.7	77	4000
CH_4											
Variation of fuel gas concentration											
M-1	880	1.4	20						10.2	597	518
M-2	880	1.5	20						10.7	597	518
M-3	880	1.9	15						10.2	448	691
M-4	880	2.8	10						10.2	299	1036
M-5	880	5.6	5						10.2	149	2072
Lower FR temperature											
M-6	830	1.3	20						9.4	597	518
M-7	830	1.5	15						8.0	448	691
M-8	830	2.6	10						9.4	299	1036
M-9	830	5.2	5						9.4	149	2072
Syngas CO/H_2 = 1											
Variation of fuel gas concentration											
S-1	880	1.9	78		39.0	8.2	6.8	39.0	13.6	761	406
S-2	880	1.8	64		31.8	8.2	6.8	31.8	10.2	621	498
S-3	880	3.3	45		22.5	8.2	6.8	22.5	13.3	439	705
Syngas CO/H_2 = 3											
Variation of solids circulation rate (f_s)											
S-4	880	1.3	69		51.8	4.3	10.7	17.3	8.4	701	441
S-5	880	1.6	69		51.8	4.3	10.7	17.3	9.7	701	441
S-6	880	2.0	69		51.8	4.3	10.7	17.3	12.4	701	441

[(a)] N_2 to balance

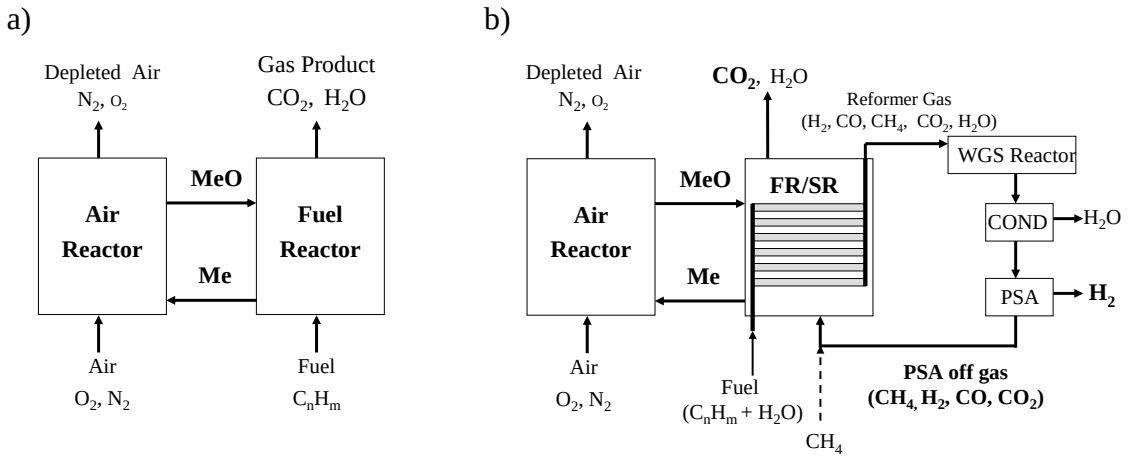

Figure 1. Schematic diagram of (a) CLC and (b) SR-CLC

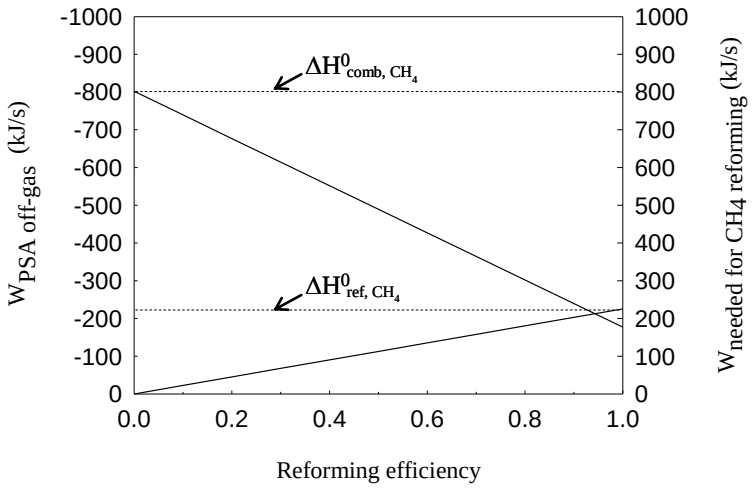

Figure 2. Power required for the reforming of methane and power supplied by combustion of the PSA tail gas as a function of the reforming efficiency. The ratio $CO:H_2:CO_2$ was assumed to be 1:1.4:2.5. The fraction of CH_4 was determined by the reforming efficiency.

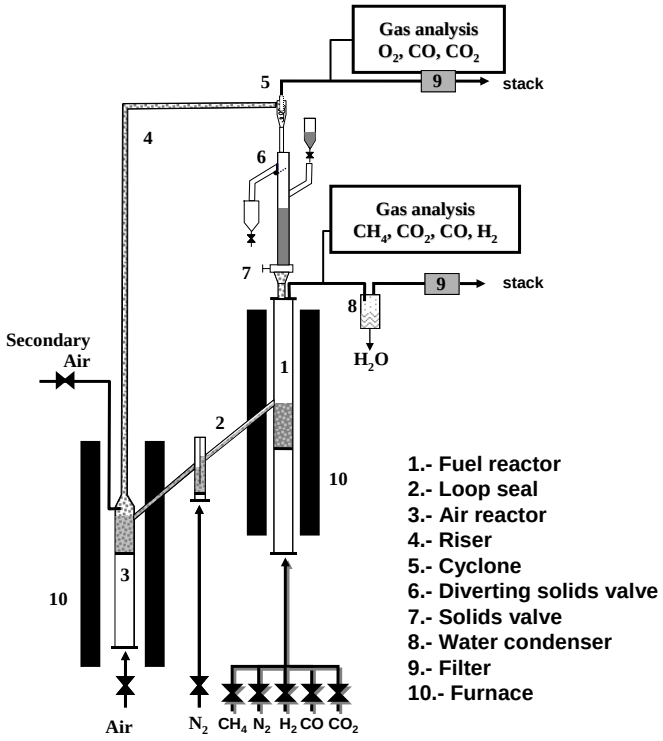

Figure 3. Schematic diagram of the 500 W_{th} Chemical-Looping Combustion facility.

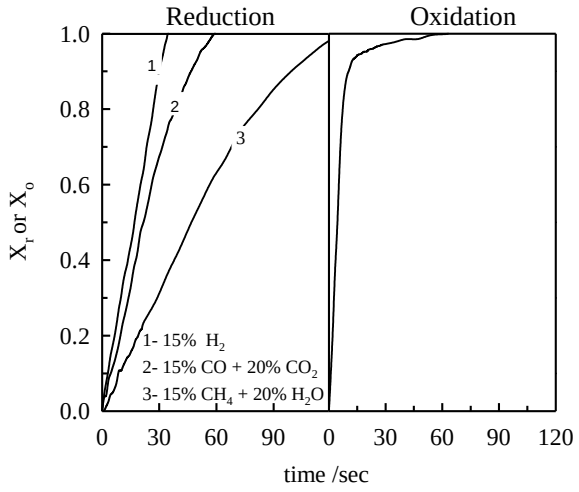

Figure 4. Conversion versus time curves of calcined oxygen carrier using H_2, CO or CH_4 as reacting gases for reduction period and air during oxidation period. T = 880 ºC.

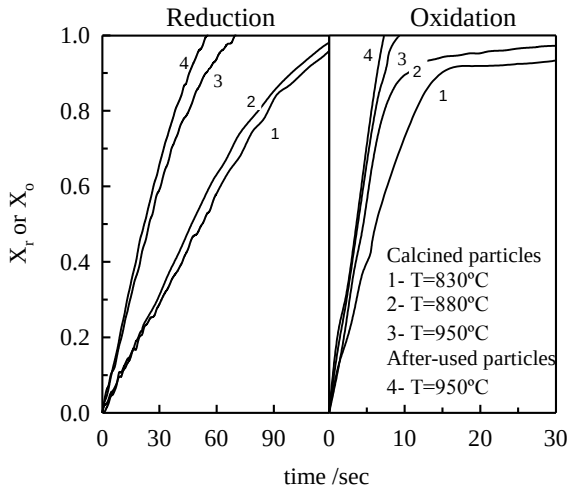

Figure 5. Conversion vs. time curves of the calcined oxygen carrier at several reacting temperatures and conversion curve at 950 ºC for particles after 111 h in the CLC facility. Reacting gas for reduction period: 15 vol.% CH_4, 20 vol.% H_2O, nitrogen to balance. Oxidation by air.

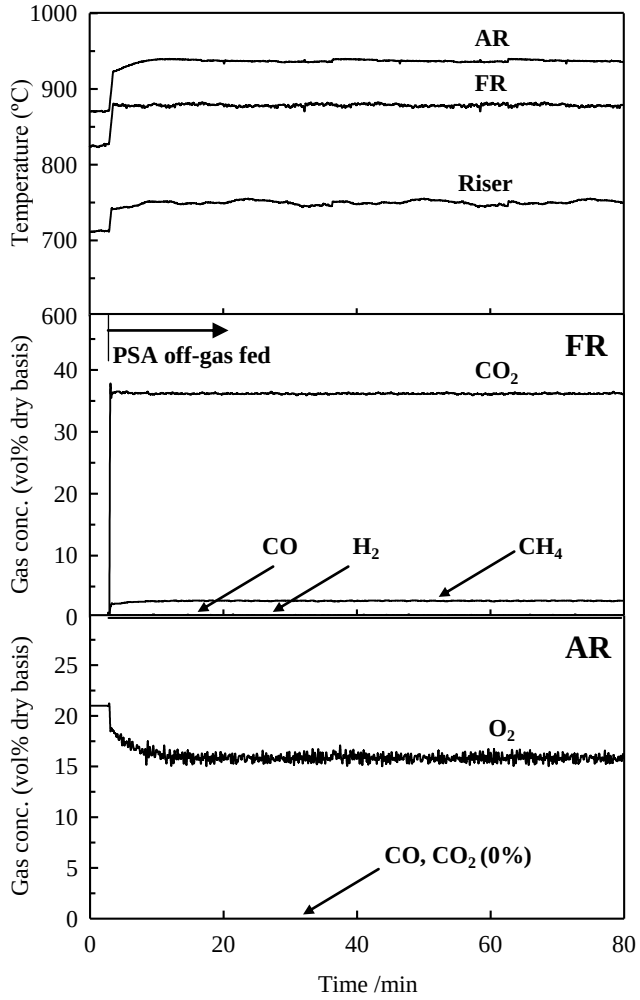

Figure 6. Temperature and gas product distribution at the outlet of AR and FR during a typical experiment. Experimental test PSA-4: T_{FR} = 880ºC, T_{AR} = 940ºC, PSA off-gas = 50 vol %, f_S = 6.6 kg h^{-1}, ϕ = 1.6.

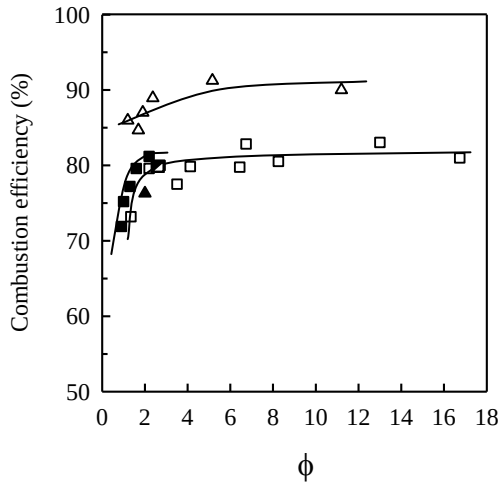

Figure 7. Effect of the oxygen-to-fuel ratio on the combustion efficiency in the fuel reactor. T=880ºC, PSA off-gas. Solids inventory in the fuel reactor 310 g: (■) variation of the solids circulation rate, (□) variation of the fuel flow. (▲) Experiment PSA-23. Solids inventory in the fuel reactor 620 g: (∆) variation of the fuel flow.

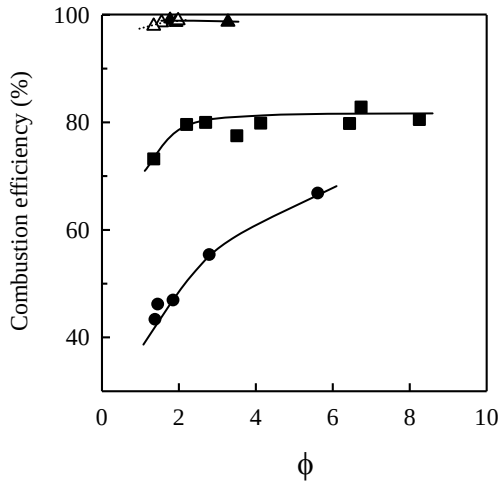

Figure 8. Effect of the fuel composition on the combustion efficiency. T=880ºC. (●) CH_4, (■) PSA off-gas, (▲) Syngas CO/H_2= 1, (∆) Syngas CO/H_2= 3.

a)

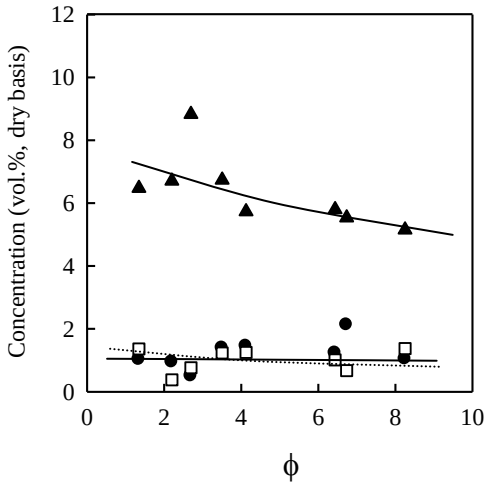
Concentration (vol.%, dry basis)
12
10
8
6
4
2
0
0
2
4
6
8
10
ϕ

b)

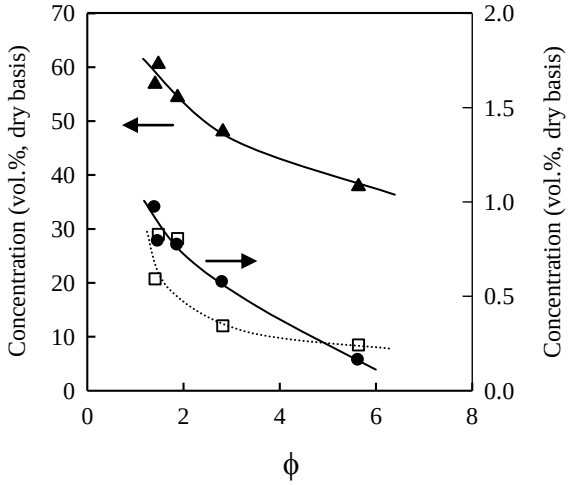
Concentration (vol.%, dry basis)
70
60
50
40
30
20
10
0
2.0
1.5
1.0
0.5
0.0
Concentration (vol.%, dry basis)
0
2
4
6
8
ϕ

c)

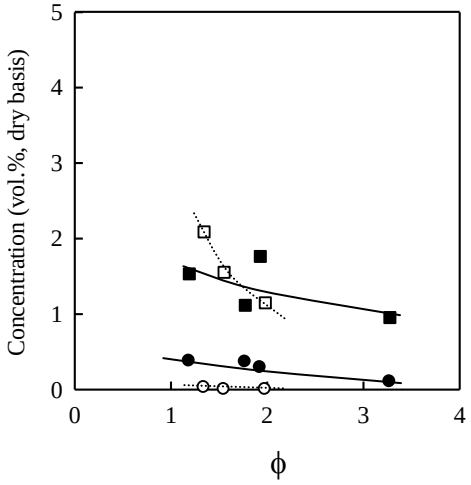
Concentration (vol.%, dry basis)
5
4
3
2
1
0
0
1
2
3
4
ϕ

Figure 9. Effect of the oxygen carrier-to-fuel ratio on the outlet gas of the FR using as fuel (a) PSA off-gas, (b) CH_4, and (c) syngas. T = 880ºC. (▲) CH_4, (●) H_2, (□) CO. Syngas: Empty dots: CO/H_2= 3, Filled dots: CO/H_2= 1. Gas concentrations are in dry basis and nitrogen free.

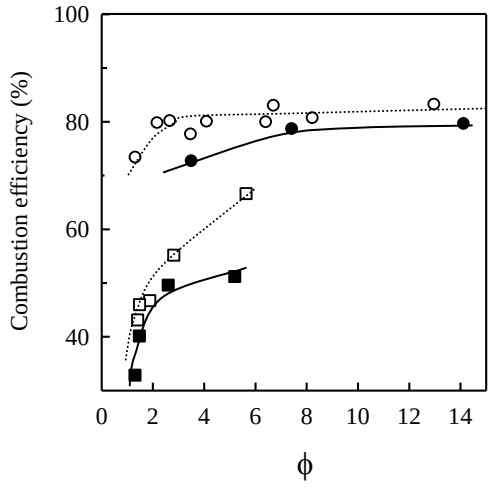

Figure 10. Effect of the fuel reactor temperature on the combustion efficiency. PSA off-gas: (●) T=830 ºC, (○) T=880 ºC. CH_4: (■) T=830 ºC, (□) T=880 ºC.

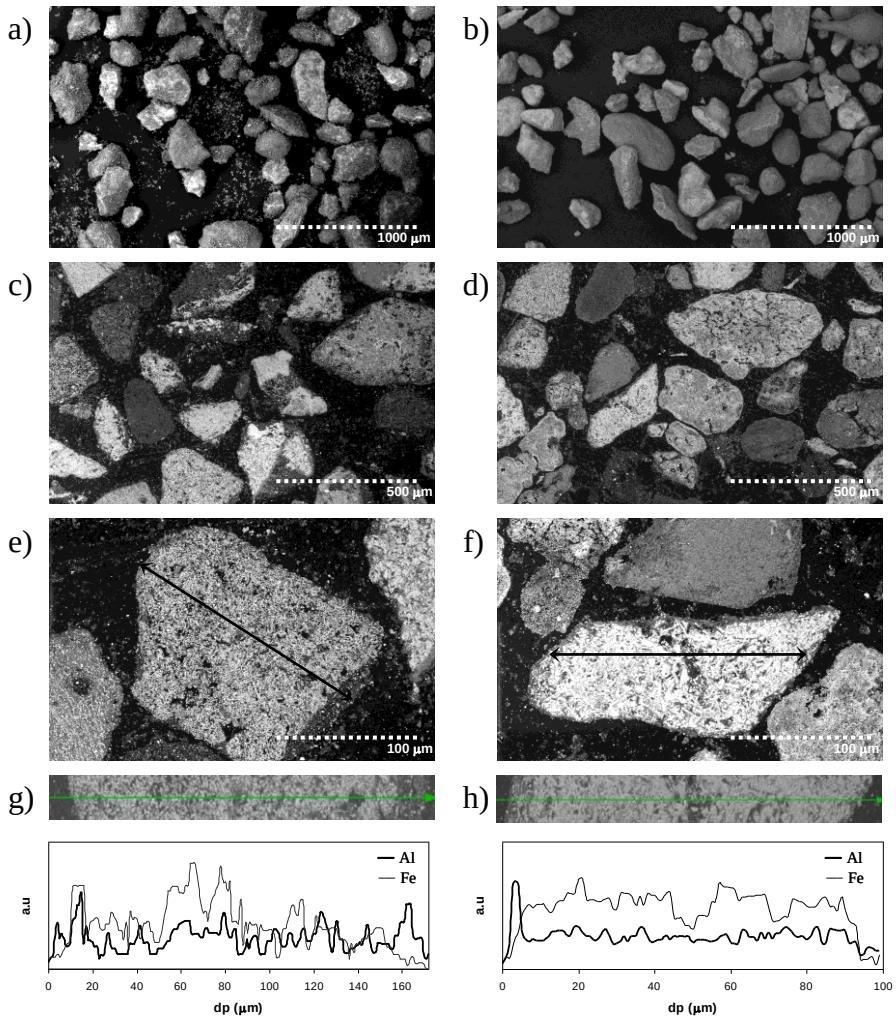

Figure 11. SEM-EDX images of the oxygen carrier particles both fresh (left) and after 111 h of operation (right); (a) and (b) SE (secondary electrons) image of the particles; (c) and (d) BSE (back-scattering electrons) photograph of a particle; (e) and (f) BSE image of a cross section of a particle; (g) and (h) EDX line profiles of Fe and Al in a cross section of a particle.